CLM-P870

CLM-P870

Virtual Particle Electromagnetic Particle-Mesh Algorithms

J. W. Eastwood

CULHAM LABORATORY

AEA TECHNOLOGY

CLM-P870

Virtual Particle Electromagnetic Particle-Mesh Algorithms

J. W. Eastwood

Theory and Computing Division
Culham Laboratory, Abingdon
Oxfordshire OX14 3DB

January 8, 1990

Abstract

A new class of current conserving particle-mesh algorithms for solving the coupled relativisitic Vlasov-Maxwell set of equations is presented. These new numerical schemes offer considerable advantages over the currently used finite difference PIC methods. They are charge and energy conserving, have good dispersive properties and are computationally fast. Their finite element derivations allow them to be applied to complex geometries more readily than their finite difference PIC counterparts. The local nature of their discretised equations is ideally suited to massively parallel computer architectures.

In this paper, an outline of the general derivation is given. One and two dimensional cases are treated in some detail, and the extension to three dimensions is discussed. Procedures for lumping and noise reduction (using a transverse current adjustment - TCA), both of which result in substantial speedups, are outlined. The name 'virtual particle' arises from an interpretation of the current assignment scheme.

Contents

1 Introduction

The particle-mesh (PM or PIC) approach has long been established as an effective method of simulating the evolution of systems described by the Maxwell-Vlasov set of equations [1,2]. The new variants of particle-mesh schemes described herein were developed to meet the need for accurate and computational inexpensive simulation to be performed in conjunction with experimental work on microwave sources at Culham Laboratory. The requirements for such a device modelling code are that it must

(a) explicitly treat at least two spatial dimensions,

(b) be capable of handling awkward geometries,

(c) handle a variety of boundary conditions,

(d) have low numerical noise, and

(e) have good conservation, dispersion and numerical stability properties.

In addition, to be an effective engineering design tool, it must be computationally fast, and in this respect, local algorithms have considerable advantages on the parallel architecture machine currently available. The novel schemes presented in this paper meet all of these requirements. An implementation of the Virtual Particle method in cylindrical geometry [16] has allowed extensive 2-D simulations to be performed on a personal workstation rather than on more powerful (and more costly!) large scientific computers that earlier finite difference PIC codes require.

Much of the speed gain in the Virtual Particle schemes arises from the elimination of charge assignment and solution of Poisson's equation to correct for accumulated errors in Gauss' Law. In particle-mesh codes, the electron (or ion) phase fluid is represented by a set of Lagrangian sample points (particles) which carry mass and charge through the mesh on which fields $\mathbf{E}$ and $\mathbf{B}$. (or in some instances potentials $\mathbf{A}$ and ϕ) are defined. The particle density and motion are used to construct, by some assignment scheme, the source charge and current densities needed to integrate Maxwell's equations forward in time. Accelerations at particle locations are found by interpolation from the mesh defined fields. Usually the discrete approximations to the Maxwell-Vlasov set of equations is not charge conserving: If the time dependent Maxwell equations (Ampere's and Faraday's Laws) are used to advance $\mathbf{E}$ and $\mathbf{B}$ using currents computed from the particle dynamics, then the initial condition of Gauss' Law ($F = \nabla \cdot \mathbf{E} - \rho/\epsilon_0 \equiv 0$) is not conserved and $\nabla \cdot \epsilon_0 \mathbf{E}$, as given by the mesh defined fields, may differ significantly from the charge density ρ computed from the

particle distribution. In such circumstances, the reliability of the computations would be questionable.

Three approaches to the well-known "charge conservation" problem have been devised. The first repeatedly solves Poisson's equation to find a correction to the longitudinal component of $\mathbf{E}$ so that F is reset to zero at each timestep [3,4]. This approach gives a relatively small overhead in simple geometries where rapid elliptic solvers [1,chap.6] can be employed, but becomes a large burden (and an obstruction to exploitation of parallelism) in the complex geometries of microwave devices. Several codes, for example WAVE [5] and ZOHAR [6] successfully use this method.

The second approach to maintaining charge conservation is to add a "pseudo-current" term into Faraday's Law which has the effect of diffusing the residual error F away [2]. The pseudo-current method has the advantage of removing the need to repeatedly solve elliptic equations, but the drawback of making Faraday's Law parabolic, thus complicating the treatment of boundary conditions and introducing a diffusion parameter which may alter the physics.

The third alternative, which is used in the schemes proposed in this paper, is to devise a current assignment scheme which ensures that some approximation to Gauss' Law is identically satisfied (to roundoff). This approach was first proposed by Buneman[9] using an impulse approximation current assignment. Unfortunately his scheme appears to generate a strong noise field [2]). Another instance, using a fraction timestepping approach, is discussed by Morse and Nielsen[11] and is used in the ISIS code[8]. More recently, Villasenov and Buneman[9] have proposed a less noisy current conserving scheme based on area weighting assignment[10].

The existing algorithms most closely related to the ones proposed in this paper are the energy conserving schemes devised by Lewis [1,12,13]. Indeed, in the limit $\Delta t \rightarrow 0$, the new Virtual Particle schemes described below reduce to Lewis' Schemes. The crucial difference is extension of the finite element formulation to the time coordinate. It is this factor which leads to exact charge conservation ($i.e. F \equiv 0$ for all t). The resulting algorithms are similar to those of Villasenov and Bunemann. Indeed, the current assignment scheme proposed in [9] is mathematically equivalent to the 'Virtual Particle' current assignment scheme for the case of linear support functions in Cartesian geometry. The finite element derivation of the Virtual Particle method has the advantages that it specifies an optimal (in the sense of Least Action) combination of current assignment/force interpolation and field solver prescriptions, and it is more general: it can be used to gives schemes in arbitrary coordinate systems, or using higher order and/or various element shapes and connectivities.

In this paper we shall focus on relatively straightforward illustrations in Cartesian geometry - other instance are discussed elsewhere [16,17]. Section 2 gives the set of differential equations to be solved, followed in section 3 by an outline of their variational finite element discretisation. An important factor to note in section 3 is the method of prescribing the local support functions for potentials in terms of a common support function S: this ensures exact charge conservation and thence leads to fast computations by eliminating the need to compute charge densities and longitudinal electric field corrections at each timestep.

The Virtual Particle scheme most similar to existing PIC schemes is that arising when S is linear on a rectangular net of elements. It is this case which has been used in Section 4 to illustrate the practical details of the derivation of the discrete equations, and to provide a link to the more commonly used finite difference approach. In section 5, the discussion of higher order charge conserving current assignment schemes has been restricted to one dimension to avoid excessive algebra. Comments on the relaxation of restrictions assumed in this paper and concluding remarks are given in the final section of the paper.

2 The Mathematical Model

The electromagnetic fields evolve according to the Maxwell equations

$$\frac{\partial \mathbf{B}}{\partial t} = -\nabla \times \mathbf{E} \tag{2.1}$$

$$\frac{\partial \mathbf{D}}{\partial t} = \nabla \times \mathbf{H} - \mathbf{j} \tag{2.2}$$

subject to initial conditions

$$\nabla \cdot \mathbf{D} = \rho \tag{2.3}$$

$$\nabla \cdot \mathbf{B} = 0 \tag{2.4}$$

where

$$\mathbf{D} = \epsilon_0 \mathbf{E}, \tag{2.5}$$

$$\mathbf{B} = \mu_0 \mathbf{H} \tag{2.6}$$

and the symbols have their usual meanings [14]. The electron phase fluid evolves according to the relativistic Vlasov equation

$$\frac{\partial f}{\partial t} + \frac{\mathbf{p}}{\mathbf{m}} \cdot \frac{\partial f}{\partial \mathbf{x}} + \mathbf{F} \cdot \frac{\partial f}{\partial \mathbf{p}} = 0 \tag{2.7}$$

whose characteristics are the equations of motion

$$\dot{\mathbf{x}} = \mathbf{v} \tag{2.8}$$

$$\dot{\mathbf{p}} = \mathbf{F} = q(\mathbf{E} + \mathbf{v} \times \mathbf{B}) \tag{2.9}$$

where $\mathbf{x}$ is position, $\mathbf{v}$ is velocity, $\mathbf{p}$ is momentum, m is mass, $\mathbf{p} = m\mathbf{v} = \gamma m_0 \mathbf{v}$, and

$$\gamma = \frac{1}{(1-(v/c)^2)^{1/2}} = \left(1 + \frac{p^2}{(m_0 c)^2}\right)^{1/2} \tag{2.10}$$

The first two moments of the one particle distribution function f give respectively the charge and current densities:

$$\rho = q \int f d^3p; \tag{2.11}$$

$$\mathbf{j} = q \int f \dot{\mathbf{x}} d^3p \tag{2.12}$$

A similar set of equations apply to ion phase fluids. For clarity, we consider only a single species (electrons) here.

If the distribution function is represented by a set of sample points (i.e. "superparticles")

$$f(\mathbf{x}, \mathbf{p}, t) = \sum_g N_s \delta(\mathbf{x} - \mathbf{x}_g(t)) \delta(\mathbf{p} - \mathbf{p}_g(t)) \tag{2.13}$$

where $(\mathbf{x}_g, \mathbf{p}_g)$; $g \epsilon [1, N_p]$ are the coordinates of the N_p superparticles, each of mass $M = N_s$ m_0 and charge $Q = N_s q$, then the Maxwell-Vlasov set may be written in terms of the action integral

$$I = \int dt d\tau \left(\frac{\mathbf{D} \cdot \mathbf{E} - \mathbf{B} \cdot \mathbf{H}}{2} - \rho\phi + \mathbf{j} \cdot \mathbf{A} \right) - \int \sum_g \frac{Mc^2}{\gamma_g} dt \tag{2.14}$$

where

$$\mathbf{B} = \nabla \times \mathbf{A} \tag{2.15}$$

$$\mathbf{E} = -\nabla\phi - \frac{\partial \mathbf{A}}{\partial t} \tag{2.16}$$

Treating I as a functional of the vector potential $\mathbf{A}$, the scalar potential ϕ and particle coordinates $\{\mathbf{x}_g\}$ leads to Euler-Lagrange equations which reduce to Maxwell's equations and the relativistic equations of motion. More extensive discussions of this are given in references [12,13,15]. The charge conservation property follows from the divergence of Eq.(2.2) and the time derivation of Eq.(2.3) :

$$\frac{\partial \rho}{\partial t} = -\nabla \cdot \mathbf{j} \tag{2.17}$$

If our numerical scheme identically satisfies this equation, then Eq.(2.3) will be true for all time provided that it is satisfied initially.

3 The Discrete Equations

The discrete approximations to Eqs.(2.1)-(2.13) are obtained by substituting finite element approximations for potentials ϕ and $\mathbf{A}$, and particle coordinates $\mathbf{x}_g$ into Eqs.(2.14)-(2.16) and taking variations with respect to the unknown potential and particle position nodal amplitudes. For simplicity, we shall assume local support functions satisfy Eq.(2.8) and Eqs.(2.15) and (2.16) exactly. More generally, we could consider weighted residual approximations to these equations.

3.1 The Field Equations

The first integral in Eq.(2.14) is the integral of the field Lagrangian density. Its variations with respect to potentials give the inhomogeneous Maxwell equations. To ensure Eqs.(2.15) and (2.16) are satisfied everywhere, we assume there exist a local-support function S associated with nodes labelled $(\mathbf{p}, n)$ on a space-time lattice,

$$S = S_{\mathbf{p},n}(\mathbf{x}, t) \tag{3.1}$$

and that support functions T, U, $V_i and W_i$ are related to derivatives of S by linear operators Δ_t and Δ_i by

$$\frac{\partial S}{\partial t} \equiv -\Delta_t U \tag{3.2}$$

$$\frac{\partial S}{\partial x_i} \equiv -\Delta_{(i)} W_{(i)}, \tag{3.3}$$

$$\frac{\partial^2 S}{\partial x_i \partial t} \equiv \Delta_t \Delta_{(i)} V_{(i)} \tag{3.4}$$

$$\frac{\partial^2 S}{\partial x_j \partial x_k} \equiv \Delta_k \Delta_j T_i \qquad i \neq j \neq k \tag{3.5}$$

Operators Δ_i and Δ_t act on the node indices p_i and n, respectively, where i labels the spatial and node label coordinates; x_i and p_i respectively. (Δ_t and Δ_i are analogues of finite difference operators). Summation is implied over repeated indices unless the indices are enclosed in braces.

The finite element approximations to the potentials are

$$\phi = \Phi U \tag{3.6}$$

$$\mathrm{A}_i = A_{(i)} W_{(i)} \tag{3.7}$$

where Φ and A are nodal amplitudes. Eq.(3.6) is a shorthand notation for

$$\phi(\mathbf{x},t) = \Phi_{\mathbf{p},n} U_{\mathbf{p},n}(\mathbf{x},t)$$

and similarly for A_i. Substituting Eqs.(3.6) and (3.7) into Eqs.(2.15) and (2.16) gives

$$B_i = \epsilon_{ijk}\frac{\partial \mathrm{A}_k}{\partial x_j} = \epsilon_{ijk}\frac{\partial W_k}{\partial x_j}A_k \tag{3.8}$$

$$\begin{aligned} E_i &= -\frac{\partial \phi}{\partial x_i} - \frac{\partial \mathrm{A}_i}{\partial t} \\ &= -\Phi\frac{\partial U}{\partial x_i} - A_{(i)}\frac{\partial W_{(i)}}{\partial t} \end{aligned} \tag{3.9}$$

Similarly, substituting them in Eq.(2.14) gives stationary points:

$$\frac{\partial I}{\partial \Phi} = \int dt d\tau \left[-D_i\frac{\partial U}{\partial x_i} - \rho U\right] = 0 \tag{3.10}$$

$$\frac{\partial I}{\partial A_i} = \int dt d\tau \left[-D_{(i)}\frac{\partial W_{(i)}}{\partial t} - H_k\epsilon_{kj(i)}\frac{\partial W_{(i)}}{\partial x_j} + j_{(i)}W_{(i)}\right] = 0 \tag{3.11}$$

Inspection of the nodal equations (3.8) - (3.11) reveal a number of conservation properties: From Eqs.(3.8) and (3.9) it follows that $\nabla\cdot\mathbf{B} \equiv 0$ and $\dot{\mathbf{B}} \equiv -\nabla\times\mathbf{E}$ for the discrete system. Taking Δ_t of Eq.(3.10) and summing Δ_i of Eq.(3.11) over i give two expressions for the discrete approximation to $\partial(\nabla\cdot\mathbf{D})/\partial t$. These two expressions are identical provided that

$$\int dt d\tau \left[\rho\frac{\partial S}{\partial t} + j_i\frac{\partial S}{\partial x_i}\right] \equiv 0 \tag{3.12}$$

Substituting from Eqs. (2.11) - (2.13) for ρ and $\mathbf{j}$, and using $S = 0$ at the limits of the integral show Eq. (3.12) to be true. This implies that if Eq. (3.11) is used to update $\mathbf{D}$, the approximation Eq. (3.10), to $\nabla\cdot\mathbf{D} - \sigma \equiv 0$, will be true (to roundoff) for all times provided it is satisfied initially. All the examples considered below have this property.

An expression for field energy conservation can be obtained from Eq.(3.11) by multiplying by nodal field amplitudes E_i and summing over spatial node indices:

$$\int dt d\tau \left(\mathbf{D}\cdot\Delta_t\bar{\mathbf{E}} + \mathbf{H}\cdot\frac{\partial\bar{\mathbf{B}}}{\partial t} + \mathbf{j}\cdot\bar{\mathbf{E}}\right) = 0 \tag{3.13}$$

where $\bar{E}_i = W_i E^i$, and $\dot{\bar{B}}_i = -\epsilon_{ijk}\partial\bar{E}_k/\partial x_j$.

3.2 The Particle Equations

It follows from Eqs.(2.11) - (2.14) that the contribution to the action integral of some particle g is

$$I_g = \int dt \left[-Q\phi + Q\dot{\mathbf{x}} \cdot \mathbf{A} - \frac{Mc^2}{\gamma} \right] \tag{3.14}$$

Let the ℓ – th component of the position of the particle, x_ℓ be approximated by

$$x_\ell = x_\ell^n X^n(t) \tag{3.15}$$

and $v_\ell = \dot{x}_\ell$, then

$$\frac{\partial I_g}{\partial x_\ell^n} = \int dtQ \left[-\frac{\partial \phi}{\partial x_k} + v_m \frac{\partial A_m}{\partial x_k} \right] \frac{\partial x_k}{\partial x_\ell^n} \tag{3.16}$$

$$+ \int dt \left[Q \left(\frac{\partial v_{im}}{\partial x_\ell} \right) A_m + \gamma M v_m \frac{\partial v_m}{\partial x_\ell^n} \right] = 0 \tag{3.17}$$

Integrating the first term in the second integral of Eq.(3.17) by parts gives

$$\frac{\partial I_g}{\partial x_\ell^n} = \int dtQ \left[-\frac{\partial \phi}{\partial x_\ell} - \frac{\partial A_\ell}{\partial t} + v_m \left(\frac{\partial A_m}{\partial x_\ell} - \frac{\partial A_\ell}{\partial x_m} \right) \right] X^n + \int dt \gamma M v_\ell \dot{X}^n = 0 \tag{3.18}$$

i.e.

$$\int dt \left[Q \left(\mathbf{E} + \mathbf{v} \times \mathbf{B} \right)_\ell X^n + p_\ell \dot{X}^n \right] = 0 \tag{3.19}$$

3.3 The Virtual Particles

The prescriptions for assigning charge and currents from particles to the mesh are given by the source terms in Eqs.(3.10) and (3.11):
Charge assignment

$$\begin{aligned} q_{\mathbf{p},n} &= \int dt d\tau \rho U_{\mathbf{p},n}(\mathbf{x}, t) \\ &= \int dt \sum_g Q_g U_{\mathbf{p},n}(\mathbf{x}_g(t), t) \end{aligned} \tag{3.20}$$

current assignment

$$\begin{aligned} I_i &= \int dt d\tau j_{(i)} W_{(i)} \\ &= \int dt \sum_g Q_g \dot{x}_{(i)} g W_{(i)}(\dot{\mathbf{x}}_g(t), t) \end{aligned} \tag{3.21}$$

Where $x_{(i)g}$ is the $i - th$ component of the position of the g – th particle. Eqs.(3.20) and (3.21) are integrals over piecewise polynomials in t. Such integrals are given exactly

using Gaussian quadrature [18]. The support assignment functions U and W correspond to the assignment functions of conventional finite difference/particle methods. It is these observations which led to the concept of Virtual Particles: Gaussian quadrature exactly computes integrals of polynomials of degree n by taking a weighted sum of the integrand evaluated at the n Gaussian quadrature points. The difference between these new schemes and conventional ones is that current is assigned in the usual fashion, but from "virtual" particles distributed at Gaussian points along the trajectory segments betwen the timelevels at which particle coordinates are stored, and with velocities proportional to the segment lengths in each element.

4 A 2-D Cartesian TM Model

The lowest order form of S which allow Eqs.(2.15) and (2.16) to be exactly satisfied is piecewise linear in all coordinates. We shall use this choice in a two dimensional Cartesian transverse magnetic (TM) model to illustrate the practical realisation of the method outlined in section 3. On a uniform net of elements, this choice leads to a numerical scheme very similar to that using the standard interlaced TM finite difference net [2].

4.1 The Field Equations

For clarity, we shall work with units which give length unity sides to elements and $\mathbf{E} = \mathbf{D}, \mathbf{B} = \mathbf{H}$. On a regular array of elements, S becomes a product of triangle functions, where for a node with global indices ℓ, m, n

$$S^{n-1/2}_{\ell,m}(x,y,t) = \Lambda_\ell(x)\Lambda_m(y)\Lambda^{n-1/2}(t) \tag{4.1}$$

Indices ℓ, m, n respectively label in the x, y and t directions, and the triangle function is defined as

$$\Lambda_k(z) = \Lambda(z-k) = \begin{cases} 1-|z-k| & ; \quad |z-k|<1 \\ 0 & ; \quad \text{otherwise} \end{cases} \tag{4.2}$$

The other support functions (U, V_i, W_i, T_i) are similar products of triangle and top hat (Π) functions:

$$\Pi(z) = \begin{cases} 1 & ; \quad -1/2 < z \leq 1/2 \\ 0 & ; \quad \text{otherwise} \end{cases} \tag{4.3}$$

Let us now consider single element contributions to Eqs.(3.10) and (3.11). Variables are either piecewise constant (C) or piecewise linear (L) over elements, as summarised in Table 1. Figure 1 shows the node locations on the element. Note that if a regular array of

such elements are assembled, one obtains the interlaced TM meshes used in finite difference schemes [2]. To interpret Table 1, consider for example the electric fields E_x and E_y. Using the cardinal labelling shown in Fig.1c and assuming the point $(x, y) = (0, 0)$ is at the south west corner, the components of the field are

$$E_x = E_N y + E_S(1 - y) \tag{4.4}$$

$$E_y = E_E x + E_W(1 - x) \tag{4.5}$$

and similarly for other entries in the table. For the south west node $U = U_{SW} = (1-x)(1-y)$ giving the contribution to Eq.(3.10) for the SW node

$$\Delta\left(\frac{\partial I}{\partial \Phi_{SW}}\right) = 1/6(2E_E + 2E_S + E_N + E_W) - \int dtdxdy\rho U_{SW} \tag{4.6}$$

(Fields scale as fluxes in Eq.(4.6) i.e., for elements of sides $\Delta x, \Delta y$, replace E_x by $E_x \Delta y$ and E_y by $E_y \Delta x$.)

Figure 2 illustrates diagramatically the multipliers of the electric field node amplitudes for U_{SW}, U_{NW}, U_{NE} and U_{SE}. Shown against nodes are six times the node amplitude multiplier. Assembling the contributions of the four elements gives the global discrete approximation to Gauss' Law prescribed by Eq.(3.10) for node ℓ, m as

$$\partial_x(\alpha_y E_x) + \partial_y(\alpha_x E_y) = q \tag{4.7}$$

where difference operator ∂_x and ∂_y (and averaging operators α_x and α_y) respectively act on the indices ℓ and m:

$$\partial_x f_{\ell,m} = f_{\ell+1/2,m} - f_{\ell-1/2,m} \tag{4.8}$$

$$\alpha_x f_{\ell,m} = (f_{\ell-1,m} + 4f_{\ell,m} + f_{\ell+1,m})/6 \tag{4.9}$$

and similarly for ∂_y and α_y on index m. In Eq.(4.7), for node ℓ, m

$$q = q_{\ell,m} = \int dtdxdy\rho U_{\ell,m} \tag{4.10}$$

and all terms have the same time index n. Repeating the above exercise for Eq.(3.11) gives node amplitude multipliers as shown schematically in Fig.3, and assembling contributions from adjacent elements on a uniform net give the discrete approximations to the components of Faraday's Law

$$\partial_t(\alpha_y E_x) = \partial_y(\alpha_t B_z) - I_x \tag{4.11}$$

$$\partial_t(\alpha_x E_y) = -\partial_x(\alpha_t B_z) - I_y \tag{4.12}$$

where,

$$I_x = I^{n+1/2}_{x\ell+1/2,m} = \int dtdxdyW_1 j_x \tag{4.13}$$

$$I_y = I^{n+1/2}_{y\ell,m+1/2} = \int dtdxdyW_2 j_y \tag{4.14}$$

The remaining field equations (3.8) and (3.9) can also be expressed in operator notation for node amplitudes:-

$$B_z = \partial_x A_y - \partial_y A_x \tag{4.15}$$

$$E_x = -\partial_x \phi - \partial_t A_x \tag{4.16}$$

$$E_y = -\partial_y \phi - \partial_t A_y \tag{4.17}$$

$$\Rightarrow \partial_t B_z = \partial_y E_x - \partial_x E_y \tag{4.18}$$

Note that these equations for the fields differ from the usual finite difference equations only in the appearances of the averaging operators in Eqs.(4.7), (4.11) and (4.12).

4.2 The Particle Equations

The expression Eq.(3.19) for the discrete approximation to the equation of motion assumes that particle positions vary continuously in time (by setting X^n to a triangle function) and this leads to implicit equations of motion. From a computational cost viewpoint, such a scheme is unattractive.

In general, the timestep in explicit electromagnetic calculations is controlled by the Courant condition on the field equations. Consequently, we can employ lower order approximations in the particle orbit calculations with little loss of accuracy. This approach is adopted here. Instead of assuming particle positions vary linearly from timelevel $n-1/2$ to $n+1/2$, we take it constant over the interval, so $\mathbf{x} = \sum_n \Pi^n(t)\mathbf{x}^n$, then to evaluate Eq.(3.19) we set $\mathbf{v} = \bar{\mathbf{v}}$ to yield the usual finite difference expression

$$\mathbf{p}^{n+1/2} - \mathbf{p}^{n-1/2} = Q\Delta t \left[\mathbf{E}^n(\mathbf{x}^n) + \bar{\mathbf{v}}^n \times \frac{(\mathbf{B}^{n+1/2} + \mathbf{B}^{n-1/2})}{2}\right] \tag{4.19}$$

where

$$\bar{\mathbf{v}}^n = (\mathbf{v}^{n+1/2} + \mathbf{v}^{n-1/2})/2 \tag{4.20}$$

and

$$\mathbf{x}^{n+1} = \mathbf{x}^n + \mathbf{v}^{n+1/2}\Delta t \tag{4.21}$$

The fields at particle locations are the value of the finite element fields at that point. Thus, for this example, E_x is the NGP in x and CIC in y interpolant of the nodal values, E_y is CIC/NGP and B_z is NGP/NGP (cf. Table 1, with $L \Rightarrow$ CIC, $C \Rightarrow NGP$).

4.3 Charge and Current Assignment

The charge and current assignment schemes for this example are given by evaluating Eqs.(4.10) and (4.13)-(4.14) respectively. For the impulse approximation to the motion ($\mathbf{x} = \Pi^n(t)\mathbf{x}^n$), the contribution of a single particle to ρ in time interval $t^{n-1/2} < t < t^{n+1/2}$ is $Q\delta(\mathbf{x} - \mathbf{x}^n)\Pi^n(t)$, so the contribution of the particle to $q^n_{\ell,m}$ is, by Eq.(4.10)

$$\delta q^n_{\ell,m} = QU^n_{\ell,m}(\mathbf{x}^n) \tag{4.22}$$

and since U is linear in x and y, (cf.Table 1), Eq.(4.22) simply states that charge assignment is by the CIC or Area Weighting scheme [1,2].

Evaluation of Eq.(4.13) and (4.14) for the impulse approximation is treated as a limiting process, assuming a particle moves linearly from $\mathbf{x}^n$ to $\mathbf{x}^{n+1}$ in some small time interval $\tau = t - t^{n+1/2} \in (-\epsilon/2, \epsilon/2)$ and letting $\epsilon \to 0$. From Eqs.(2.12), (2.13) and (4.13), the current contribution of a single particle is

$$\delta I_x = \int Q dt \dot{x} W_1(\mathbf{x}(t), t) \tag{4.23}$$

where $\mathbf{x} = \sum_n \Pi^n(t)\mathbf{x}^n$

For $\tau (\in (-\epsilon/2, \epsilon/2))$

$$\mathbf{x} = \frac{\mathbf{x}^{n+1} - \mathbf{x}^n}{\epsilon} = \frac{\mathbf{v}^{n+1/2}}{\epsilon}\tau \tag{4.24}$$

Hence Eq.(4.23) becomes

$$\delta I_x = \int_{-\epsilon/2}^{\epsilon/2} Q d\tau \frac{v_x^{n+1/2}}{\epsilon} W\left(\mathbf{x}^n + \frac{\mathbf{v}^{n+1/2}(\tau + \epsilon/2)}{\epsilon}\tau\right) \tag{4.25}$$

Substituting $s = \tau/\epsilon$ and letting $\epsilon \to 0$ gives

$$\delta I_x = \int Q ds v_x^{n+1/2} W_1(\mathbf{x}(s), 0) \tag{4.26}$$

Similarly, from Eq.(4.14)

$$\delta I_y = \int Q ds v_y^{n+1/2} W_2(\mathbf{x}(s), 0) \tag{4.27}$$

Eqs.(4.26) and (4.27) give the current assignment prescription which satisfies charge conservation,

$$\partial_t q = -\partial_x I_x - \partial_y I_y \tag{4.28}$$

when q is accumulated using CIC. Note that from Eqs.(4.7), (4.11) and (4.12) this charge conservation property is unaffected by lumping any of the averaging operators acting on components of $\mathbf{E}$ and or $\mathbf{B}$.

Eqs.(4.26) and (4.27) prescribe current assignment as the path integral of mixed NGP/CIC current assignment from points along the line from $\mathbf{x}^n$ to $\mathbf{x}^{n+1}$. If points $\mathbf{x}^n$ and $\mathbf{x}^{n+1}$ lie in the same element, the integrand is a linear function, and the integral is equal to the integrand evaluated at the midpoint. For a path crossing element boundaries, the contribution to each element is given by the integrand evaluated at the midpoint of the trajectory segment in that element. Figure 4 illustrates the charge and current assignment from a single particle. The current assignment scheme corresponding to area weighting charge assignment from a unit charge in a unit side element:-

$$\delta\rho_{NE} = xy \tag{4.29}$$

$$\delta\rho_{NW} = (1-x)y \tag{4.30}$$

$$\delta\rho_{SE} = x(1-y) \tag{4.31}$$

$$\delta\rho_{SW} = (1-x)(1-y) \tag{4.32}$$

is

$$\delta I_N = \bar{y}\Delta x \tag{4.33}$$

$$\delta I_S = (1-\bar{y})\Delta x \tag{4.34}$$

$$\delta I_E = \bar{x}\Delta y \tag{4.35}$$

$$\delta I_W = (1-\bar{x})\Delta y \tag{4.36}$$

where $\bar{x} = (x_f + x_i)/2, \bar{y} = (y_f + y_i)/2$, $\Delta x = x_f - x_i, \Delta y = y_f - y_i$. Points (x_i, y_i) and (x_f, y_f) are respectively the start and end points of the trajectory segment in the finite element.

4.4 Lumping

The evolutionary equations for the electromagnetic fields, Eqs. (4.11), (4.12) and (4.18) require matrix inversion at each step to invert the averaging operators. Lumping the time averaging operator (i.e. $\alpha_t B_z \rightarrow B_z$) reduces the matrix inversion to tridiagonal solutions to find E_x and E_y from $\alpha_y E_x$ and $\alpha_x E_y$. Lumping has no effect on Gauss' Law (Eq.(4.7)) and the charge conservation property, but does degrade accuracy.

Extending lumping to the space averaging operators α_x and α_y leads to further reductions in the computational work at the cost of further degredation of accuracy, but conservation laws for charge and energy still exist (cf. section 4.5). The main benefit of lumping is that the computations become completely local: there are no matrix inversions or Poisson equations to solve. Such schemes are particularly attractive for implementation on parallel architecture computers.

A measure of numerical stability and of the loss of accuracy due to lumping is given by wave dispersion analysis. A plane electromagnetic wave, in vacuo, satisfies the dispersion relation $\omega^2 = k_x^2 + k_y^2$ where ω is frequency and $\mathbf{k} = (k_x, k_y)$ is wavenumber (c = 1 is assumed). The corresponding dispersion relation for the finite element equations is obtained by Fourier transforming Eqs.(4.11), (4.12) and (4.18) with $I_x = I_y = 0$:-

$$\omega^2 F(\pi\omega/\omega_g) = k_x^2 F(\pi k_x/K_x) + k_y^2 F(\pi k_y/K_y) \tag{4.37}$$

where for elements of sides $\Delta_x, \Delta_y, \Delta_t$ in the x, y and t direction, respectively

$$\omega_g = \frac{2\pi}{\Delta_t}, K_x = \frac{2\pi}{\Delta_x}, K_y = \frac{2\pi}{\Delta_y} \tag{4.38}$$

and

$$F(\theta) = \frac{\sin^2\theta}{\theta^2\left[1 - 2/3\sin^2\theta\right]} \tag{4.39}$$

Equation (4.37) can be parameterised in terms of the mesh aspect ratio $\alpha = \Delta_y/\Delta_x$, the Courant number $C = \Delta_t/\Delta$ and the wavevector direction $\phi = \arctan(k_y/k_x)$ to give $\Omega = \Omega(\kappa, \alpha, C, \Phi)$ where $\Omega = \omega/2\omega_g$, $\kappa = |\mathbf{k}|/2k_g$ and $k_g/2\pi = 1/\Delta = \sqrt{\left[1/\Delta_x^2 + 1/\Delta_y^2\right]}$. In the absence of discretisation effects, $\Omega = \kappa$. The dependence of α, C and Φ give a measure of numerical error.

For numerical stability, the frequency ω (or Ω) must be real which, by Eq.(4.37), implies $C \leq 1$. Figure 5a shows the dispersion curves for wave propagation on a square mesh using a typical practical Courant number $C = 0.5$. The curves are drawn only for the first Brillouin zone of the numerical mesh. They show a small angular dependence $\Omega(\kappa, \Phi = 0) \neq \Omega(\kappa, \Phi = 45^o)$ and increase in wave velocity ($\Omega > \kappa$) due to the discretisation. However, for wavelength greater than $4\Delta_x$ numerical errors are small.

Figures 5b and 5c show the effects lumping. Lumping only $\alpha_t B_z$ (figure 5b) causes an increase in phase velocity, whilst lumping all three averages reduces phase velocity and increases angular anisotropy. The case shown in figure 5c is equivalent to the standard TM interlaced finite difference approximation [2]. One difficulty introduced in case 5c is that the wave phase velocity is subluminous: the numerical mesh is behaving as a slow wave

structure, introducing the possibility of numerical Cerenkov instability [19]. Note in figure 5b that the lumping of B, which is equivalent to adding a solenoidal current, increases phase velocity. This point is exploited in TCA (cf section 4.7).

4.5 Energy Conservation

The lumped approximations to the field equation retain an exact conservation law. Defining, the averaging in time operators $\mathbf{A}$ and $\mathbf{G}$ by

$$(\mathbf{A}_t f)^{n+1/2} = (f^{n+1} + f^n)/2 \tag{4.40}$$

$$(\mathbf{G}_t f^2)^n = f^{n+1/2} f^{n-1/2} \tag{4.41}$$

and defining similar space averaging operator $\mathbf{A}_x$ and $\mathbf{A}_y$, we may write the energy conservation law for the lumped (in space and time) scheme in terms of nodal amplitudes:-

$$\sum \left(\partial_t (\mathbf{A}_y \frac{E_x^2}{2} + \mathbf{A}_x \frac{E_y^2}{2} + \mathbf{G}_t \frac{B_z^2}{2}) + \mathbf{A}_y (I_x A_t E_x) + \mathbf{A}_x (I_y A_t E_y) \right) = 0 \tag{4.42}$$

The sum in Eq.(4.42) is taken over all elements. Poynting fluxes at the surfaces are included by means of surface currents in the ohmic terms.

The impulse approximation to the particle equations of motion, Eq.(4.19), also has an exact conservation law for the kinetic energy. Dotting Eq.(4.19) with $\mathbf{p}^{n+1/2} + \mathbf{p}^{n-1/2}$, rearranging and summing over particles, g, gives

$$T^{n+1/2} - T^{n-1/2} = \sum_g \frac{(\mathbf{p}^{n+1/2} + \mathbf{p}^{n-1/2}) \cdot \mathbf{E}^n}{(\gamma^{n+1/2} + \gamma^{n-1/2})} \tag{4.43}$$

Note however that Eqs.(4.42) and (4.43) do not imply exact energy conservation (to round-off). This is because the impulse approximation used in the particle equations of motion lead to an ohmic exchange term which is not identical to the ohmic exchange term in the field energy conservation law. The discrepancy gives a measure of time truncation errors.

4.6 Charge Conservation

The charge conservation property, Eq.(4.28) causes Eq.(4.7) (or its lumped approximation) to be satisfied for all time if it is initially satisfied and if fields are advanced using Eqs.(4.11) and (4.12) (or their lumped equivalents). The method of derivation of charge and current assignment ensures charge conservation: this can be verified directly by using Eqs.(4.29)-(4.36) for particles in a single element, and assembly the results. The proof is a little more elegant in terms of the assignment functions. The (CIC) charge assigned to a particular node at a given timelevel from a single particle of charge unity is

$$q = \Lambda(x)\Lambda(y) \tag{4.44}$$

Differencing over one timestep gives

$$\begin{aligned}
\partial_t q &= \Lambda(x+v_x)\Lambda(y+v_y) - \Lambda(x)\Lambda(y) \\
&= \int_0^1 ds \frac{\partial}{\partial s}\Lambda(x+sv_x)\Lambda(y+sv_y) \\
&= \int_0^1 dsv_x\Lambda'(x+sv_x)\Lambda(y+sv_y) \\
&+ \int_0^1 dsv_y\Lambda(x+sv_x)\Lambda'(y+sv_y)
\end{aligned} \tag{4.45}$$

But $\Lambda'(x) = -\partial_x\Pi(x), \Lambda'(y) = -\partial_y\Pi(y)$. Therefore

$$\begin{aligned}
\partial_t q &= -\partial_x \int_0^1 dsv_x\Pi(x+sv_x)\Lambda(y+sv_y) \\
&- \partial_y \int_0^1 dsv_y\Lambda(x+sv_x)\Pi(y+sv_y) \\
&= -\partial_x I_x - \partial_y I_y \text{ by Eqs.(4.26) and (4.27)}
\end{aligned} \tag{4.46}$$

4.7 Noise Control using TCA

The algorithms derived using the variational time centred formulation are lossless, apart from radiation and particle fluxes through the boundaries. The small number of simulation superparticles and discountinuous current assignment (cf. section 5.2) enhances current fluctuations above those in the physical counterpart. The radiation field noise energy depends on all past fluctuations and can rapidly mask collective phenomena being studied. The obvious expedients of increasing the number of particles and refining the current assignment are unattractive because of larger computational costs. The transverse current adjustment (TCA) scheme described below allows computations to be successfully undertaken with particle numbers which in its absence would be too small to keep noise levels acceptable.

The idea behind TCA is to introduce a dissipative solenoidal current, $\mathbf{j}_d$, which attenuates noise generated by particle graininess but leaves collective modes and charge conservation unaffected. One choice which has proved both simple and effective is

$$\mathbf{j}_d = |\beta|\,\nabla_d \times \nabla_d \times \mathbf{E}(\equiv -|\beta|\,\nabla_d \times \Delta_t B) \tag{4.47}$$

where ∇_d is the discrete gradient operator and Δ_t is the backward time difference operator. Equation (4.47) may be interpreted physically as a consequence of a lossy medium or numerically as a small adjustment to the time centring of the magnetic field. It adds an energy loss term

$$\sum |\beta|\,\Delta_t B_z A_t \partial_t B_z \tag{4.48}$$

to the power balance equation (4.42).

TCA is most simply implemented by precomputing an additional current given by Eq.(4.47 The effect of the TCA term on dispersion for the lumped case is shown in Figure 6. TCA introduces a multiplicative factor $(1 + \beta(1 - exp(-i2\pi\omega/\omega_g)))$ on the r.h.s. of Eq.(4.37), causing solutions for Ω to be complex. Plotted in figure 6 are Ω_r (solid) and Ω_i/β.

The stability criterion, with lumped space and time averaging operators and TCA becomes

$$C^2(1 + 2\beta) < 1 \tag{4.49}$$

The best approach to combining noise control with good dispersion appears to be to choose some small β to suppress nonphysical noise effects, then set the largest timestep to satisfy Eq.(4.49). Figure 6b shows one such case, with $\beta = .05$ and $C = 0.9$: this gives good dispersion at small k, and damps the poorly represented large k modes. Illustration of the effectiveness of TCA is given elsewhere [16]. Typical, a coefficient of $\beta \simeq .01$ (corresponding to a 1% shift from exactly timecentring β in Ampere's Law equations) is sufficient.

5 1-D Electrostatic Models

In one dimension the longitudinal (electrostatic) and transverse (electromagnetic) components of the field separate respectively parallel to and transverse to the spatial mesh. In this case, the methods outlined in the previous section can be applied directly to the one dimensional electrostatic and/or electromagnetic particle model, with the interesting result that Poisson's equation needs solving only once to initialise a calculation.

5.1 CIC charge assignment

Linear support functions in the variational finite element formulation lead to the usual energy conserving 1-D electrostatic model [1]. For particles of unit charge on a unit spaced mesh, the charge assigned to node p from particle g is

$$\delta q_p = \Lambda(x_g - p) = \Lambda_p(x_g) \tag{5.1}$$

amd the electric field E satisfies

$$E_{p+1/2} = \phi_{p-1} - \phi_p \tag{5.2}$$

where

$$\phi_{p-1} - 2\phi_p + \phi_{p+1} = -q_p \tag{5.3}$$

From Eq.(5.1),

$$\begin{aligned}\partial_t(\delta q_p) &= \Lambda_p(x_g + v_g) - \Lambda_p(x_g) \\ &= \int_0^1 dt \frac{\partial}{\partial t}\Lambda_p(x_g + v_g t) \\ &= \int_0^1 v_g dt \Lambda_p'(x_g + v_g t) \\ &= -\partial_x \int_0^1 dt v_g \Pi(x_g + v_g t) \end{aligned} \tag{5.4}$$

Substituting Eq.(5.2) into (5.3), differencing in time and using Eq.(5.4). gives

$$\partial_t \partial_x E = -\partial_x I_x \tag{5.5}$$

where

$$I_x = \int_0^1 dt v_g \Pi(x_g + v_g t) \tag{5.6}$$

Summing Eq.(5.5) in x gives

$$\partial_t E = I_0 - I_x \tag{5.7}$$

where the constant of summation I_0 (the return current) is determined by the boundary conditions. Eqs.(5.6) and (5.7) provide the basis for a novel (but equivalent to standard schemes[1]) method of stepping forward the 1-D electrostatic model in time:

Timestep loop.

i) update positions for particles $g = 1, N_p$

$$x_g^{n+1} = x_g^n + {v_g}^{n+1/2} \tag{5.8}$$

ii)compute currents at nodes $p + 1/2$

$$\begin{aligned} I_{p+1/2}^{n+1/2} = \sum_{i=1}^{N_p} & \max \left[p, \min(p+1, x_g^{n+1})\right] \\ & - \max \left[p, \min(p+1, x_g^n)\right] \end{aligned} \tag{5.9}$$

iii) compute return current

e.g for fixed voltage b.c.

$$I_0^{n+1/2} = \frac{1}{N} \sum_{p=1}^{N} I_{p+1/2}^{n+1/2} \tag{5.10}$$

iv) advance fields

$$E_{p+1/2}^{n+1} = E_{p+1/2}^n + \left(I_0^{n+1/2} - I_{p+1/2}^{n+1/2}\right) \Theta^2 \tag{5.11}$$

where Θ^2 is a dimensionless factor depending on the N_p, N and Δt.
v) update velocities

$$v_g^{n+3/2} = v_g^{n+1/2} + E^{n+1}(x_g^{n+1}) \tag{5.12}$$

vi) go to i).

A similar timestep loop can be defined for 'momentum conserving' schemes, differing in that Eq.(5.2) is replaced by

$$E_p = (\phi_{p-1} - \phi_{p+1})/2, \tag{5.13}$$

Eq.(5.11) is replaced by

$$E_p^{n+1} = E_p^n + \left(I_0^{n+1/2} - (I_{p+1/2}^{n+1/2} + I_{p-1/2}^{n+1/2})\right)\Theta^2 \tag{5.14}$$

and the interpolation of E in Eq.(5.12) become CIC rather NGP.

5.2 Higher Order Schemes

A whole family of Virtual Particle schemes can be obtained in one, two and three dimensions by choosing appropriate local support functions. We illustrate the process here by considering the spline function family of schemes in one dimension. The hierarchy of charge assignment schemes CIC, TSC, PQS, etc., [1] arise from linear, quadratic, cubic spline, etc. support functions. In each case, the corresponding current assignment function is the next lowest order. Thus, on a uniform net of unit width elements, if current is assigned to nodes from a particle according to

$$I_{p+1/2} = \int_0^1 dsvW_{p+1/2}(x + sv) \tag{5.15}$$

then charge is assigned according to

$$q_p = \int \Pi(x')W_p(x - x')dx' \tag{5.16}$$

Current assignment is implemented in terms of the contributions from trajectory segments. Consider the segment from x_i to x_f in element p, as shown in Figure 7. Current assignment from that segment for the various charge assignment/current assignment combinations are as follows:

CIC charge assignment

$$\begin{aligned} I_{p-1/2} &= \int_{x_i}^{x_f} dx'\Pi_{p+1/2}(x') \\ &= x_f - x_i = \Delta x \end{aligned} \tag{5.17}$$

Eq.(5.17) gives the NGP prescription of current Δx from a virtual particle at position $\bar{x} = (x_i + x_f)/2$.

TSC charge assignment

$$\begin{aligned} I_{p-1/2} &= \bar{x}\Delta x \\ I_{p+1/2} &= (1-\bar{x})\Delta x \end{aligned} \tag{5.18}$$

This current assignment scheme can be likewise interpreted as CIC from a virtual particle at position $\bar{x}$ with current strength Δx.

PQS (cubic spline) assignment

$$\begin{aligned} I_{p-1/2} &= \int_{x_i}^{x_f} dx 1/2(1/2-x)^2 \\ I_{p+1/2} &= \int_{x_i}^{x_f} dx (3/4-x)^2 \\ I_{p+3/2} &= \int_{x_i}^{x_f} dx 1/2(1/2+x)^2 \end{aligned} \tag{5.19}$$

The quadratic integrand requires two point quadrature for exact evaluation: this is interpreted as TSC assignment from two virtual particles at $\bar{x} \pm \Delta x/\sqrt{3}$ with current strengths $\Delta x/2$. Alternatively, the integrals can be evaluated directly. One scheme, using two point quadrature for $I_{p-1/2}$ is

$$\begin{aligned} \bar{x} &= (x_f + x_i)/2 \\ \Delta x &= (x_f - x_i) \\ \bar{y} &= \bar{x} - 1/2 \\ y_1 &= \bar{y} + \Delta x/\sqrt{3} \\ y_2 &= \bar{y} - \Delta x/\sqrt{3} \\ I_{p-1/2} &= \frac{\Delta x}{4}\left[y_1^2 + y_2^2\right] \\ I_{p+3/2} &= I_{p-1/2} + \bar{x}\Delta x \\ I_{p+1/2} &= \Delta x - I_{p-1/2} - I_{p+3/2} \end{aligned}$$

giving a real arithmetic operation count of 16 per trajectory segment.

6 Final Remarks

The finite element formulation of the Virtual Particle (VP) Electromagnetic Particle-Mesh algorithms provides a systematic approach to obtaining charge conserving schemes for solving the coupled relativistic Vlasov and Maxwell equation set. These algorithms are competitive with their existing finite difference PIC counterparts in accuracy, in computational speed and storage, and in flexibility. They can be tuned for speed by restricting elements to one form, or some speed per node can be traded for flexibility in element shape and connectivity.

The emphasis in this paper has been to outline the general derivation, with simple one and two dimensional Cartesian cases used to illustrate details. The examples were chosen to show the link with conventional finite difference based schemes [1,2] and to provide easy to follow examples of procedures followed in more complex cases. Programs implementing the 1-D schemes of section 5.1 and 2-D schemes of section 4 have been used to study 1-D and 2-D diodes, magnetically insulated transmission lines (MITL) and magnetically insulated transmission line oscillators (MILO) [20,21].

More general cases and higher dimension charge conserving virtual particle algorithms will be subjects of future reports. It is apparent from the discussion of section 3 that virtual particle (VP) methods generalise straightforwardly to three dimensions, to general coordinate systems and to more general element shapes [17,20]. Already, the 2-D Cartesian scheme and program have been extended to polar coordinates to study cylindrical diodes, MITL's and MILO's [16,22,23]. Some work has been undertaken in developing 3-D schemes, where it has been shown that it is possible to express the whole timestep loop in terms of local operations on single elements or between continguous neighbouring elements [24]. This makes the VP method ideally suited to massively parallel architecture machines with neighbouring processor connectivity.

Practical details for the successful modelling of realistic devices - such as data adressing, input-output and diagnostics, treatment of awkward shaped boundaries with possible electron emission and of electromagnetic power injection and extraction - have not been dealt with here. However, they present no serious obstable, as has been illustrated by the 2-D cylindrical and Cartesian simulations referred to above.

For the problems to which the VP method has thus far been applied, numerical noise has not caused serious difficulties. Linear element current assignment, both with and without TCA, has allowed calculation to proceed for tens of thousands of timesteps without failing. If this lowest order (linear) support proves inadequate for more noise sensitive situations, then the schemes of section 5.2 or their multidimensional equivalent can be used, but with the obvious increased cost per particle per timestep. The associated increased cost per node

point per timestep arising from higher order support functions can be avoided if desired by using lower order field representations in a weighted residual (instead of variational) derivation. The advantage of the higher order spline functions is that they reduce numerical noise. Their disadvantage is that if they implemented without lumping, they give non-local and implicit approximations which are difficult to implement in awkward geometries. It seems likely that alternatives to splines would give a better compromise in some cases, and this possibility will be the subject of a future study.

References

[1] R. W. Hockney and J. W. Eastwood, "Computer Simulation using Particles", McGraw-Hill (1980) (student edn. Adam-Hilger, 1988).

[2] C. K. Birdsall and A. B. Langdon, "Plasma Physics via Computer Simulation", McGraw-Hill (1985).

[3] J. P. Boris, Proc. 4th conf. Num. Sim. Plasmas, (N.R.L., Washington, 1971), p3.

[4] I.Haber et al., Proc. 4th Conf. Num. Sim. Plasmas (N.R.L., Washington, 1971), p.126

[5] D.W.Forslund et al., Phys. Rev. A, **11** (1975)679.

[6] A.B.Langdon and B. F. Lasinski, Meth. Comp. Phys., **16** (1976) 327.

[7] B.M.Marder, J. Comput. Phys. **68** (1987) 48.

[8] G.R.Gisler and M.E.Jones, Bull. Am. Phys. Soc. **29** (1984) 1208.

[9] O.Buneman in : Relativistic Plasmas eds. O. Buneman and W. B. Pardo (Benjamin, N.Y. 1968).

[10] J. Villasenov and O. Buneman, "Rigorous Charge Conservation for Local Electromagnetic Field Solver", to appear J. Comput. Phys. (1989).

[11] R. L. Morse and C. W. Nielsen, Phys. Fluids **14** (1971) 830.

[12] H. R. Lewis, J. Comput. Phys. 6(1970) 136.

[13] H. R. Lewis, Meth. Comp. Phys. 9 (1970) 307.

[14] J. R. Reitz and F. J. Milford, Foundations of Electromagnetic Theory. (Addison-Wesley, 1962).

[15] H. Goldstein,"Classical Mechanics". (Addison-Wesley, 1950).

[16] J. W. Eastwood and T. C. Hender, "VENUS-RZ, a 2-D relativistic electromagnetic particle-mesh code", in preparation, (1989).

[17] J. W. Eastwood, "Charge Conserving Virtual Particle Electromagnetic Particle-Mesh Schemes in General Curvilinear Coordinates", in preparation (1989).

[18] A. J. Baker, Finite Element Computational Fluid Dynamics. (McGraw-Hill, 1985) p.114.

[19] B. Godfrey, J. Comput. Phys. 15 (1974) 504.

[20] J. W. Eastwood, Underlying Research on EM Modelling, Annual Report, Culham, February 1989.

[21] J. W. Eastwood, paper SD10, IEEE Int. Conf. Plasma Sci. Seattle, May 1988.

[22] J. W. Eastwood, paper 3D1, IEEE Int. Conf. Plasma Sci., Buffalo, N.Y., May 1989.

[23] J. W. Eastwood and T. C. Hender, paper IM1 13th Conf. Num. Sim. Plasma, Santa Fe., N.M., Sept. 1989.

[24] J. W. Eastwood, paper PMA11, 13th Conf. Num. Sim. Plasma, Santa Fe, N.M., Sept. 1989.

Table 1: Support functions for the linear brick element used in the 2-D TM Cartesian example. L denotes linear and C constant over an element.

Variable	x	y	t
ϕ	L	L	C
A_x	C	L	L
A_y	L	C	L
E_x	C	L	C
E_y	L	C	C
B_z	C	C	L

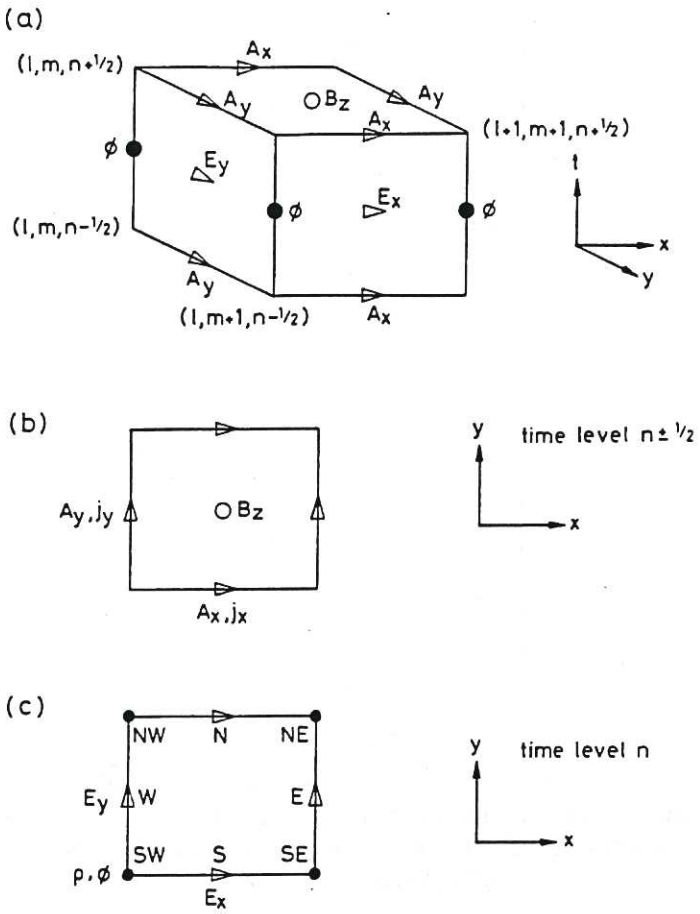

Fig. 1 The space-time finite element brick showing the location of nodes and quantities stored at those nodes. Index triplets (ℓ, m, $n-\frac{1}{2}$), etc. give the global (x, y, t) node coordinate for elements assembled in a uniform lattice.

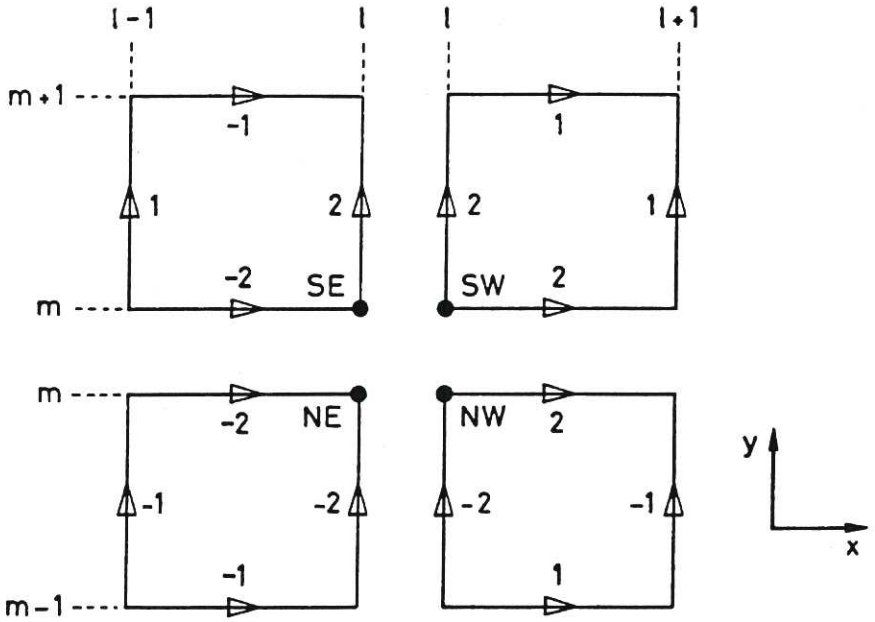

Fig. 2 Node amplitude multipliers (×6) for the electric field amplitudes in Eq.(3.10). Indices ℓ and m are global node indices.

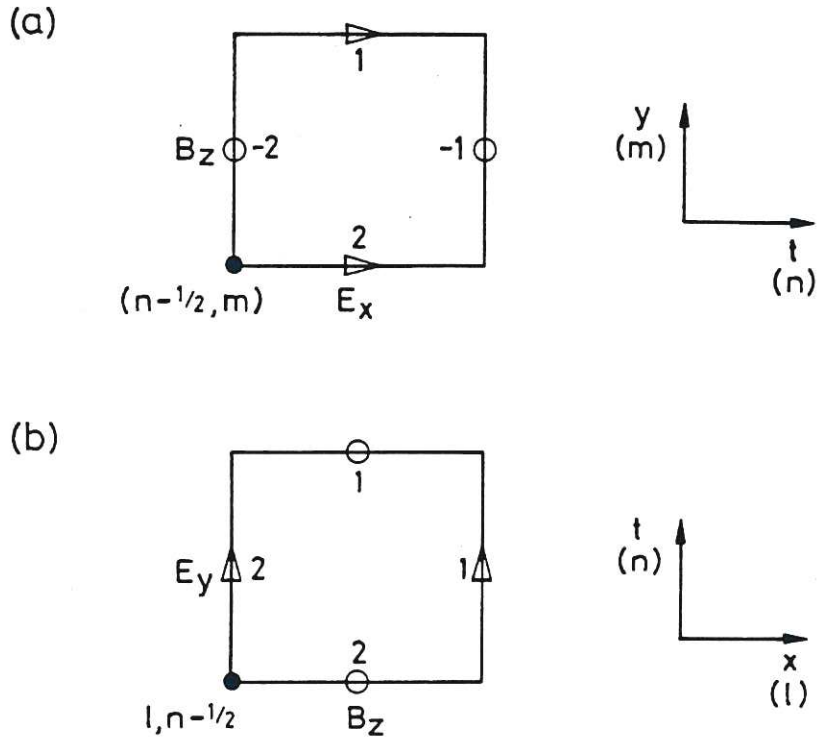

Fig. 3 Node amplitude multiplier (×6) for the electric field and magnetic field amplitudes in a) the x-component and b) the y-component of Eq.(3.11). Indices ℓ, m, and n are respectively x, y and t global indices of the nodes.

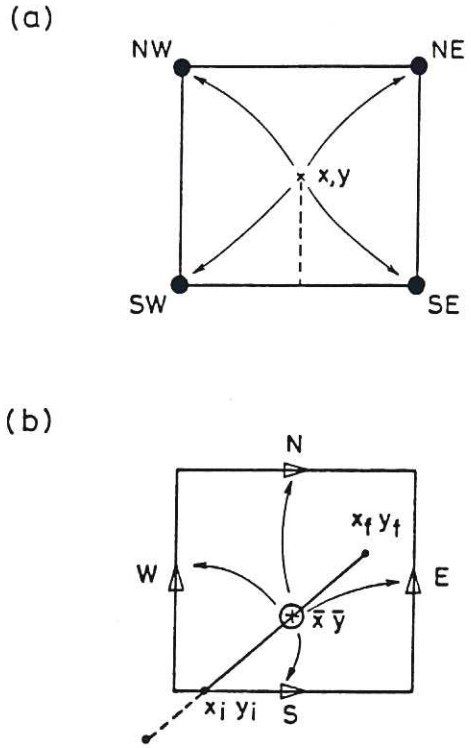

Fig. 4 a) Charge assignment from a single particle and b) current assignment from a single particle trajectory segment for a linear support function.

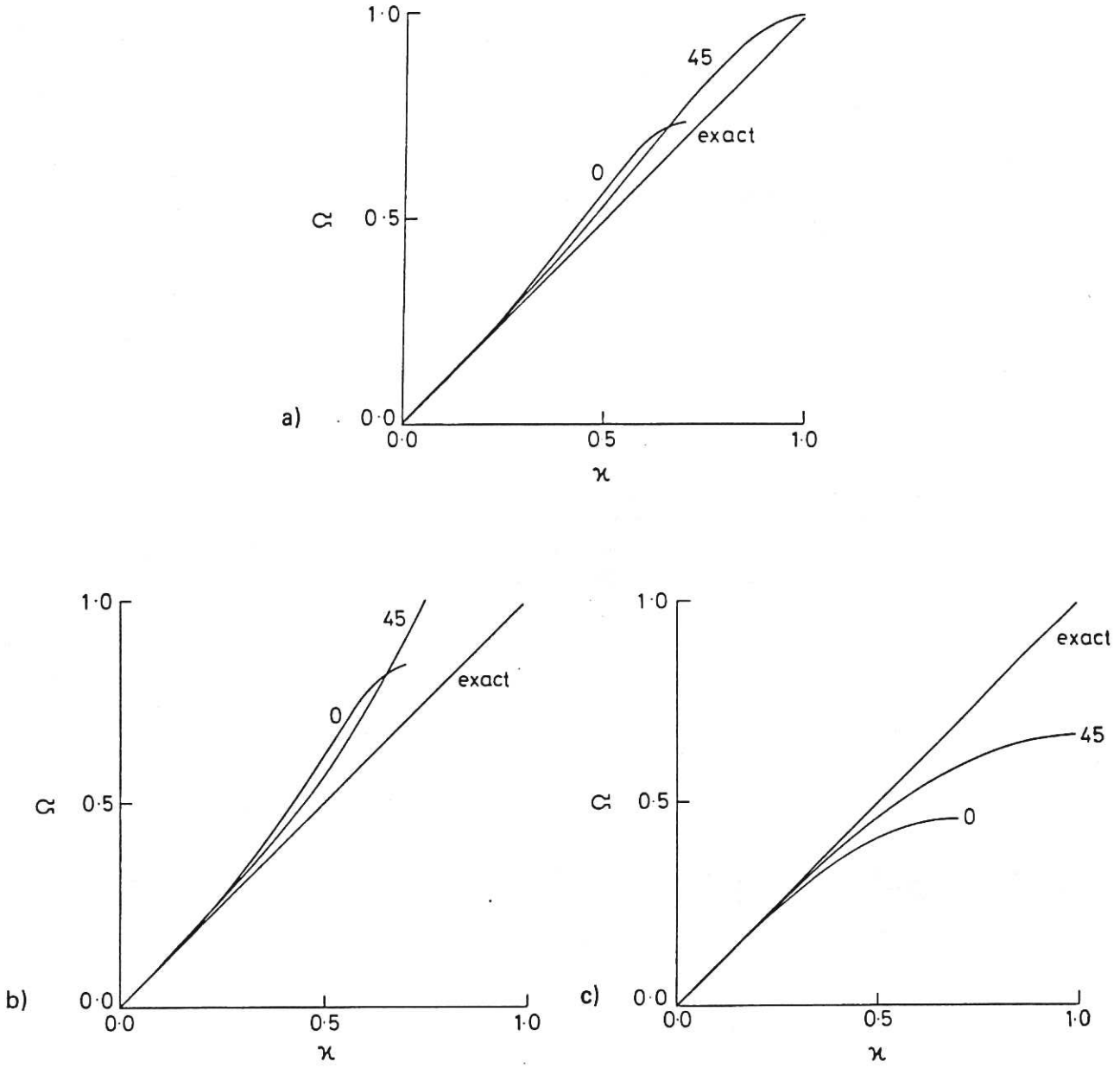

Fig. 5 a) Frequency Ω versus wavenumber κ for plane EM waves on the square lattice shown in figure 1 for wavevectors along a mesh axis (0°) and mesh diagonal (45°) using Courant number 0.5. b) As a), but with the time averaging term lumped in the discrete field equation. c) As a), but with space and time averaging terms lumped. The nodal equations are equivalent to the standard TM leapfrog finite difference equation for this case.

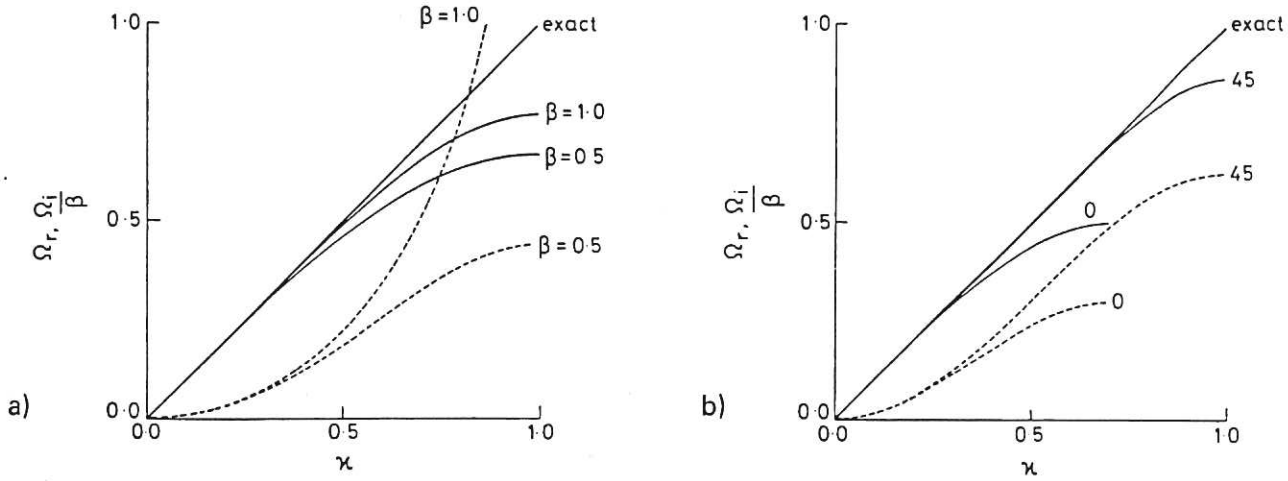

Fig. 6 a) Frequency (solid curves) and damping (broken curves) for the lumped scheme with TCA, $\beta=0.5$, and 1.0, $\theta=45°$, show that damping improves wave dispersion. b) Typical operating parameters ($C=0.9$, $\beta=0.005$) show a lumped scheme with TCA gives a good combination of accurate dispersion at long wavelength and noise damping at short wavelength.

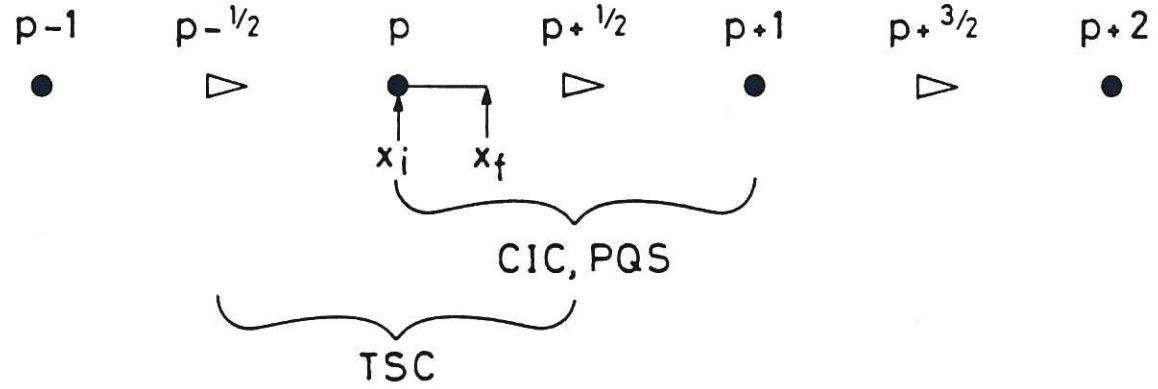

Fig. 7 Node labelling for the 1-D assignment scheme examples. Charges are stored at integral nodes (p, $p+1$, ...). Element p is centered on node $p+½$ for CIC and PQS, and on node p for TSC.